PLANT PATHOLOGY

Xanthomonas coordinates type III–type II effector synergy by activating fruit-ripening pathway

Trang Thi-Thu Phan[1]*, Rodrigo Silva Araujo Streit[2], Gerald V. Minsavage[3], Joachim Kilian[4], Paloma de los Angeles Aguilera[1], Nan Wang[1]†, Nicolas Brich[1]‡, Robert Morbitzer[1], Edda von Roepenack-Lahaye[4], Brice Charleux[5], Boris Szurek[5], Priscila Oliveira de Giuseppe[2], Concetta Licciardello[6], Jeffrey B. Jones[3], Paulo J. P. L. Teixeira[7], Gabriela Felix Persinoti[2], Mario Tyago Murakami[2], Chang Liu[1]§, Jan Grau[8], Thomas Lahaye[1]*

Plant cell walls harbor vast carbohydrate reserves, yet how pathogens unlock them remains unclear. We show that the citrus canker pathogen *Xanthomonas citri* subsp. *citri* (*Xcc*) mobilizes cell wall sugars by hijacking a fruit-ripening program through the type III effector PthA4, which activates the ripening coordinator CsLOB1. CsLOB1 induces approximately 100 genes, many encoding enzymes involved in cell wall breakdown. In the nonfruiting species *Nicotiana benthamiana*, CsLOB1 likewise promotes *Xanthomonas* growth, showing that its activity is not strictly dependent on a ripening program. Transcriptomics and reporter assays revealed PthA4-dependent activation of the *Xcc* xylan CUT system, triggered by host-derived xylose and including a type II–secreted xylanase. Thus, PthA4-driven cell wall remodeling activates bacterial xylan use, establishing a TIII–TII effector feedforward loop that fuels *Xcc* proliferation.

Bacterial plant pathogens exploit plant carbohydrates, most of which are stored in cell walls (*1*). Accordingly, many bacteria secrete cell wall–degrading enzymes (CWDEs) into the extracellular space between plant cells (the apoplast) through the type II secretion system (T2SS) (*2*, *3*). However, CWDEs also release damage-associated molecular patterns (DAMPs), which are perceived by membrane-resident pattern recognition receptors (PRRs) (*2*). To counter defenses activated by PRRs, which detect DAMPs as well as pathogen-associated molecular patterns (PAMPs), many bacteria use a type III secretion system (T3SS) to inject effectors (T3Es) that suppress immunity, resulting in effector-triggered susceptibility (ETS) (*4*).

Xanthomonas citri subsp. *citri* (*Xcc*) is the causal agent of citrus canker. This disease prompted one of the most expensive plant disease eradication programs ever attempted, involving the removal of ~16 million citrus trees between 1995 and 2006 at an estimated cost of $1.3 billion, underscoring its severe agroeconomic impact (*5*). *Xcc* virulence depends on PthA4, a transcription activator–like effector (TALE) conserved across citrus-infecting *Xanthomonas* (*6*). PthA4-deficient mutants show >100-fold reduced in planta growth, demonstrating its central role in virulence (*6*). After T3SS-mediated injection into host cells, PthA4 enters the nucleus, binds a 19–base pair (bp) effector-binding element, and activates transcription of the downstream *Citrus sinensis LATERAL ORGAN BOUNDARIES 1* (*CsLOB1*) gene (*6*). *CsLOB1* encodes a transcription factor with an N-terminal LOB domain, characteristic of the LOB transcription factor family. We reasoned that CsLOB1's native developmental role might provide clues as to why its pathogen-induced expression enhances *Xcc* virulence.

CsLOB1 binds to and activates a large set of host genes

To identify CsLOB1-regulated genes, grapefruit (*Citrus paradisi* cv. Duncan) leaves were inoculated with *Xanthomonas Xcc306* (*Xcc*), which activates *CsLOB1* through the TALE PthA4, or with a PthA4-deficient mutant (*XccΔpthA4*) (*6*). Because PthA4 also activates citrus genes beyond *CsLOB1* (*6*), we increased the specificity of the transcriptomic profiling using two designer TALEs (dTALE1 and dTALE2) targeting distinct effector-binding elements upstream of *CsLOB1* (fig. S1A). Transconjugants expressing dTALE1 (*XccΔpthA4::dTALE1)* or dTALE2 (*XccΔpthA4::dTALE2)* induced water soaking and *CsLOB1* expression like wild-type (wt) *Xcc* (Fig. 1A), showing that both dTALEs functionally replace PthA4.

For transcriptome profiling, leaves were inoculated with *Xcc*, *XccΔpthA4*, *XccΔpthA4::dTALE1*, or *XccΔpthA4::dTALE2*. RNA sequencing (RNA-seq) at 36 hours postinoculation (hpi) revealed 1437 PthA4-activated differentially expressed genes (DEGs), of which 942 (66%) were also induced by both dTALEs (see the materials and methods) (Fig. 1B and table S1). Among 1158 PthA4-repressed genes, 465 (40%) were also repressed by both dTALEs (Fig. 1B and table S1). Thus, combining PthA4 and dTALE data improves specificity for CsLOB1 target identification. Selected DEGs were already induced by 12 hpi (fig. S1B). RNA-seq at 12 hpi identified 390 up-regulated and 200 down-regulated genes, of which 216 (55%) and 76 (38%), respectively, persisted at 36 hpi (Fig. 1B and table S2). Collectively, this approach identified 216 induced and 76 repressed CsLOB1-dependent genes.

To identify direct CsLOB1 targets, we performed chromatin immunoprecipitation sequencing (ChIP-seq) using a CsLOB1-specific antibody (α-CsLOB1) (see the materials and methods) (fig. S1C). Before ChIP-seq, antibody specificity was verified by immunoblotting, detecting CsLOB1-specific signals only after expression was induced by *Agrobacterium* transfer DNA (T-DNA) in *Nicotiana benthamiana* or by *Xcc* infection in citrus, confirming high antibody selectivity (Fig. 1, C and D, and fig. S1D). We used α-CsLOB1 for ChIP-seq on *Xcc*-infected leaves, using immunoglobulin G as a control. ChIP-seq was reproducible between replicates (62% and 80% overlap at 12 and 36 hpi, respectively) (fig. S1E). CsLOB1 binding sites were enriched around transcription start sites (TSSs), spanning from 3 kb upstream to 0.2 kb downstream (Fig. 1E and fig. S1F). Within this 3.2-kb window, we identified 438 CsLOB1-bound genes at 12 hpi and 1432 at 36 hpi (Fig. 1F and table S3). Intersecting ChIP-seq and RNA-seq data identified 96 genes that were both CsLOB1 bound and transcriptionally up-regulated at both time points (Fig. 1F and table S4). None of the repressed genes showed CsLOB1 binding at either time point (Fig. 1F), indicating that CsLOB1 acts as a transcriptional activator rather than a repressor.

Sequence-specific binding of CsLOB1 to the C9G motif in vitro

To identify a CsLOB1 target motif, we analyzed 300-bp windows around ChIP-seq peaks (*7*). A 15-bp motif was found upstream of 96 transcriptionally up-regulated CsLOB1 targets (Fig. 2A) and was present in both 12- and 36-hpi replicates (fig. S2A). The motif contains conserved cytosine and guanine at positions 2 and 12 (C2 and G12), separated by a less conserved, AT-rich 9-bp spacer (Fig. 2A and fig. S2A).

Motif functionality was tested by competitive electrophoretic mobility shift assays (EMSAs) with the upstream region of the CsLOB1-regulated gene *Cs2g20600* (see the materials and methods) (fig. S2B). Mutant

[1]University of Tübingen, ZMBP - General Genetics, Tübingen, Germany. [2]Brazilian Biorenewables National Laboratory (LNBR), Brazilian Center for Research in Energy and Materials (CNPEM), São Paulo, Brazil. [3]Department of Plant Pathology, University of Florida, Gainesville, FL, USA. [4]University of Tübingen, ZMBP - Central Facilities, Tübingen, Germany. [5]Plant Health Institute of Montpellier, University of Montpellier, CIRAD, INRAE, Institut Agro, IRD, Montpellier, France. [6]Council for Agricultural Research and Economics, Research Centre for Olive, Fruit and Citrus Crops, Acireale, Italy. [7]Department of Biological Sciences, "Luiz de Queiroz" College of Agriculture (ESALQ), University of São Paulo (USP), São Paulo, Brazil. [8]Institute of Computer Science, Martin Luther University Halle-Wittenberg, Halle, Germany. ***Corresponding author. Email: thomas.lahaye@zmbp.uni-tuebingen.de (T.L.); trang.phan@zmbp.uni-tuebingen.de (T.T.-T.P.)** †Present address: Biomarker Technologies (BMKGENE), Münster, Germany. ‡Present address: Institute for Bioinformatics and Medical Informatics (IBMI), University of Tübingen, Tübingen, Germany. §Present address: Department of Epigenetics, Institute of Biology, University of Hohenheim, Stuttgart, Germany.

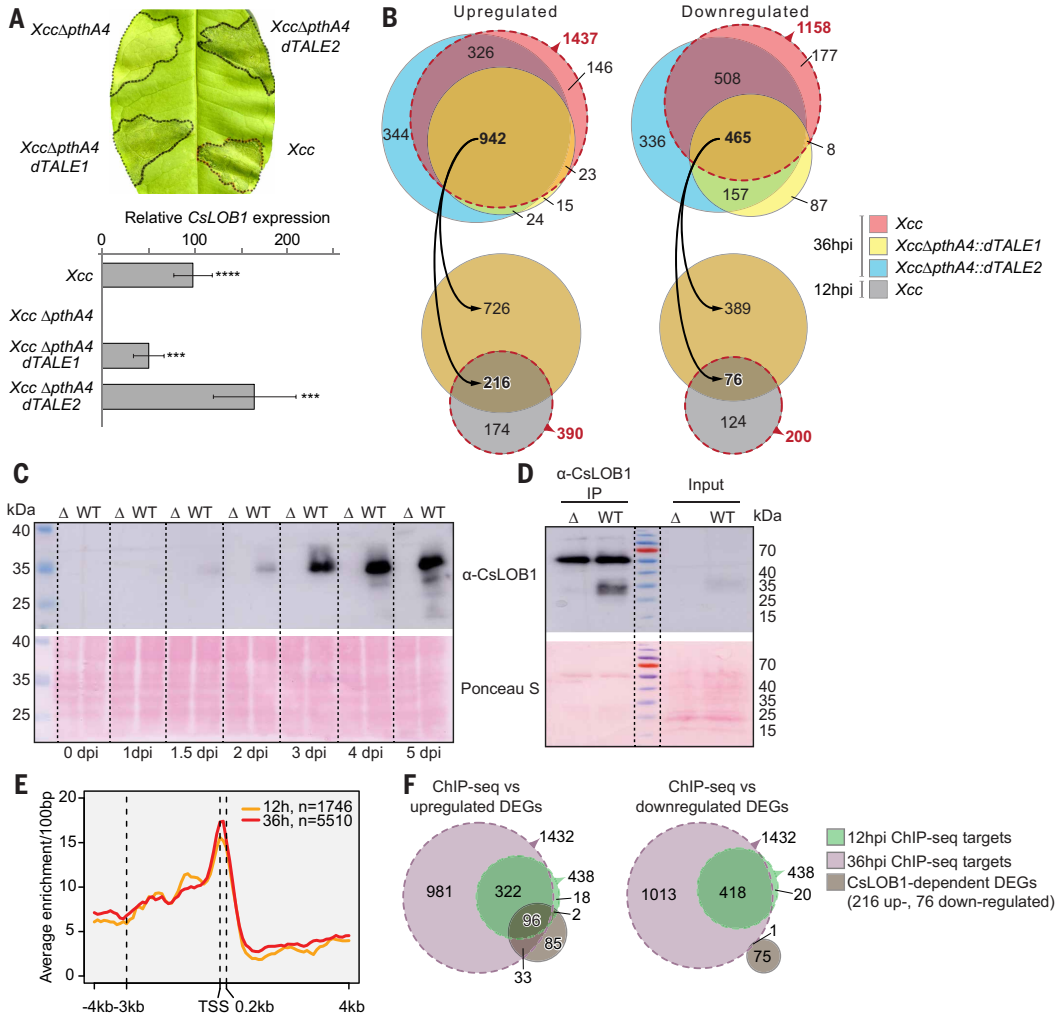

Fig. 1. RNA-seq plus ChIP-seq defines CsLOB1 regulon. (**A**) Canker symptoms and *CsLOB1* expression in grapefruit infected with *XccΔpthA4* or *Xcc* strains delivering *CsLOB1*-activating dTALEs. Dashed outlines indicate inoculated areas at 7 dpi. Bars indicate *CsLOB1* induction at 36 hours postinoculation (hpi), quantified by quantitative reverse transcription polymerase chain reaction (qRT-PCR) (normalized to *EF1α*; $n = 6$; two-tailed paired Student's *t* test; compared with *XccΔpthA4*; *** $P \leq 0.001$, **** $P \leq 0.0001$). (**B**) Size-proportional Venn diagrams of host DEGs [fold change ≥2 or ≤−2, false discovery rate (FDR) < 0.05] showing CsLOB1-dependent up and down regulons. Red font indicates PthA4-regulated gene counts; bold black indicates DEGs common to three TALEs at 36 hpi (top) and shared between both time points (bottom). (**C** and **D**) Western blot of whole tissue (C) and nuclear immunoprecipitation (IP) (D) from grapefruit leaves infected with *Xcc* ± PthA4 confirming α-CsLOB1 specificity. Blots show α-CsLOB1 signal through a CCD camera (top) with a loading control by Ponceau S (bottom). Input indicates the soluble nuclear fraction. (**E**) ChIP-seq peak density per 100-bp segment from −4 kb to +4 kb around TSSs. Dashed box defines a −3 kb to +0.2 kb annotation region. *n*, total segments overlapping ChIP-seq peaks. (**F**) Size-proportional Venn diagrams intersecting ChIP-seq–bound and RNA-seq–regulated genes (also see fig. S5).

competitors with substitutions at C2 and G12 or deletion or insertion in the AT-rich spacer failed to displace CsLOB1 from the wt probe (Fig. 2A and fig. S2C), highlighting the importance of C2, G12, and their 9-bp spacing. We designated this sequence the "C9G motif" (Fig. 2A).

The C9G motif resembles known *Arabidopsis* LOB-domain protein-binding sites (fig. S3) (*8*) but differs from reported GC-rich motifs [10-bp (GC1) and 14-bp (GC2)] in CsLOB1-induced promoters, for which direct CsLOB1 binding has not been tested (*9*). Competitive EMSAs showed that GC1 or GC2 competitors failed to displace CsLOB1 from the C9G probe, indicating lower affinity (fig. S2C). Thus, CsLOB1 specifically binds the C9G motif in vitro in a sequence- and spacing-dependent manner.

CsLOB1/2/3 activate through C9G in planta

To test C9G function in planta, a β-glucuronidase (GUS) reporter was fused to the ~1500 bp upstream region of the CsLOB1-inducible gene *Cs2g20600* containing the C9G motif (Fig. 2B). Control promoters contained mutations in one (m1) or both (mTA) conserved CG-rich regions. Only constructs with the wt C9G motif showed strong GUS activation in *N. benthamiana* leaves expressing CsLOB1 (Fig. 2B), consistent with EMSA results (Fig. 2A).

To test necessity and sufficiency, the 15-bp motif alone, a 33-bp fragment used in EMSAs, or motif-mutated variants (m1, mTA) were inserted into the tightly regulated pepper *Bs3* promoter (*10*) driving a *RUBY* reporter (*11*), which encodes enzymes for red betalain biosynthesis (Fig. 2B). Codelivery with *35S:CsLOB1* in *N. benthamiana* leaves yielded an ~8-fold higher betalain in wt versus m1 and mTA motif-mutated constructs (Fig. 2B and fig. S4A). The 15-bp and 33-bp constructs were similarly activated (Fig. 2B and fig. S4A), showing that the 15-bp C9G motif alone is sufficient for CsLOB1-dependent activation. Inserting two tandem C9G motifs into the *Bs3* promoter approximately doubled activation compared with a single motif (Fig. 2C and fig. S4B), indicating an additive effect.

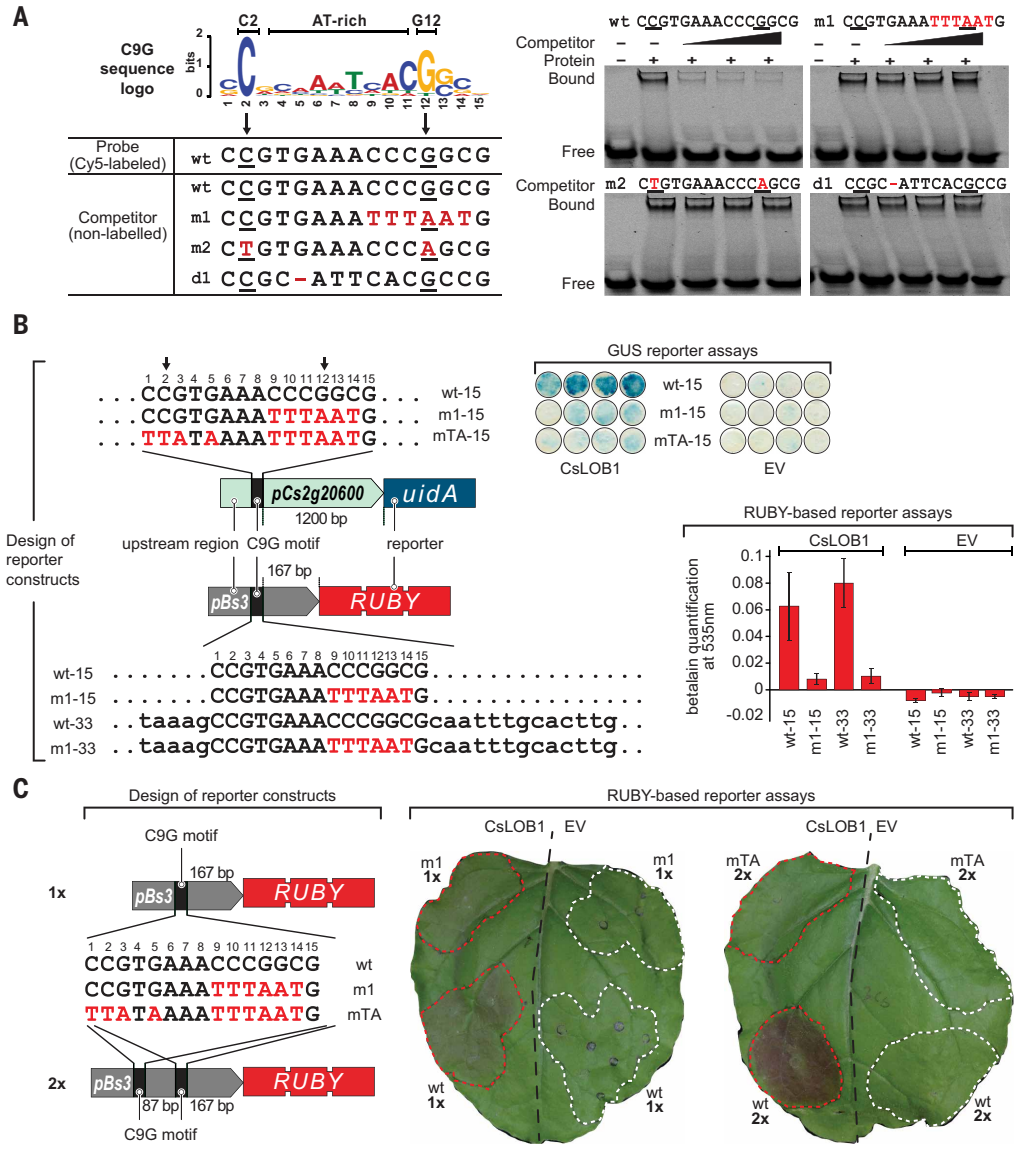

Fig. 2. A bona fide 15-bp C9G motif mediates CsLOB1 binding within target promoters. (**A**) C2 and G12 mutations in the C9G motif reduce CsLOB1 affinity in vitro. Motif logo (top) shows base frequencies across motif, predicted using MEME (*8*). C2 and G12 (arrows) indicate conserved bases with a 9-bp AT-rich spacer separating them. EMSA probes (bottom) include Cy5-labeled wt motif from *Cs2g20600*; unlabeled competitors carry red-letter mutations. Right, EMSAs using purified CsLOB1-MBP (0 or 2 μM) and 200 nM Cy5-labeled 33-bp wt probe, with unlabeled competitors at 0 (−), 25×, 50×, or 100× molar excess (triangle). (**B**) In planta recognition of C9G motif. Top, GUS assay using promoter-reporter constructs where *uidA* (GUS) is driven by 1.4-kb promoter (*P*) of *Cs2g20600* containing wt C9G (wt-15) or derivatives (m1-15 and mTA). Right, GUS activity in *N. benthamiana* at 2 dpi. Bottom, minimal pepper *Bs3* promoter (*pBs3*) with inserted C9G motifs drives RUBY reporter (*11*). (**C**) Tandem C9G motifs (2×) enhance CsLOB1-mediated activation versus single (1×) in *pBs3-RUBY*. Photo is at 42 hpi. In (B) and (C), the promoter-reporter construct was codelivered with *35S:CsLOB1-GFP* or EV. Betalain was extracted at 42 hpi and quantified photometrically at 535 nm ($n = 4$; error bars, SD).

CsLOB2 and CsLOB3 share 23 of 25 residues within the DNA-binding domain with CsLOB1 (Fig. 3A). Upon ectopic expression, both proteins promoted in planta *Xcc* growth, similar to CsLOB1 (*12*). Like CsLOB1, both preferentially activated promoters bearing the wt C9G motif, indicating highly similar or identical DNA-binding specificity (fig. S4C).

Together, these results identify C9G as a bona fide CsLOB1-binding motif that is both necessary and sufficient for CsLOB1-dependent activation and serves as a functional recognition site for the close paralogs CsLOB2 and CsLOB3 in planta.

CsLOB1/2/3 coordinate overlapping CWDE networks in leaves and fruits

Of the 96 direct CsLOB1 targets (Fig. 1F), 34 encode CWDEs, including pectate lyases and pectinesterases (fig. S5 and table S4), suggesting a native role in cell wall degradation. To gain insights into CsLOB1's native function, we analyzed public RNA-seq data across tissues (*13*, *14*) (Fig. 1). *CsLOB1* expression was low in leaves, roots, seeds, and young fruits but high in mature fruits (Fig. 3B). *CsLOB1* transcript levels were comparable in ripe fruits and *Xcc*-infected leaves, consistent with similar CsLOB1 activity in both contexts. Using a fruit tissue time-series dataset (*15*), we also analyzed CsLOB2/3. Across four tissues and six time points, CsLOB1 showed the highest overall expression, except in flavedo at 220 days after flowering, where CsLOB3 predominated (fig. S6A). These data indicate that CsLOB1 is the dominant fruit-expressed paralog and likely the main contributor to ripening among the three analyzed.

We analyzed CWDEs and their putative paralogs identified by DIAMOND reciprocal hits (*16*) in *Xcc*-infected leaves using *CsLOB1/2/3* as references for spatiotemporal expression. Hierarchical clustering of seed, leaf, and fruit transcriptomes revealed one *CsLOB1/2/3*-associated cluster of seven CWDEs preferentially expressed in mature fruits (fig. S6B). This suggests that CsLOB1 coordinates functionally equivalent CWDEs in *Xcc*-infected leaves and ripening fruits. The smaller number of CWDEs in ripening fruit likely reflects the more complex regulatory landscape of fruit ripening compared with ectopic CsLOB1 activity in leaves. Another possible factor is ripening-associated DNA hypermethylation (*17*), which may reduce CsLOB1's access to upstream C9G motifs. Thus, CsLOB1 deploys overlapping CWDE programs in infection and ripening, with fruit DNA hypermethylation potentially fine-tuning activity through reduced C9G access.

CsLOB1 and SlLOB1 share spatiotemporal patterns and DNA-binding specificity

CsLOB1's expression pattern mirrors that of the tomato (*Solanum lycopersicum*) transcription factor SlLOB1, which peaks at the onset of ripening and induces expression of CWDEs (*18*). High sequence conservation in the LOB domain between CsLOB1 and SlLOB1 (Fig. 3, A and C, and fig. S7A) suggests similar or identical DNA-binding specificity.

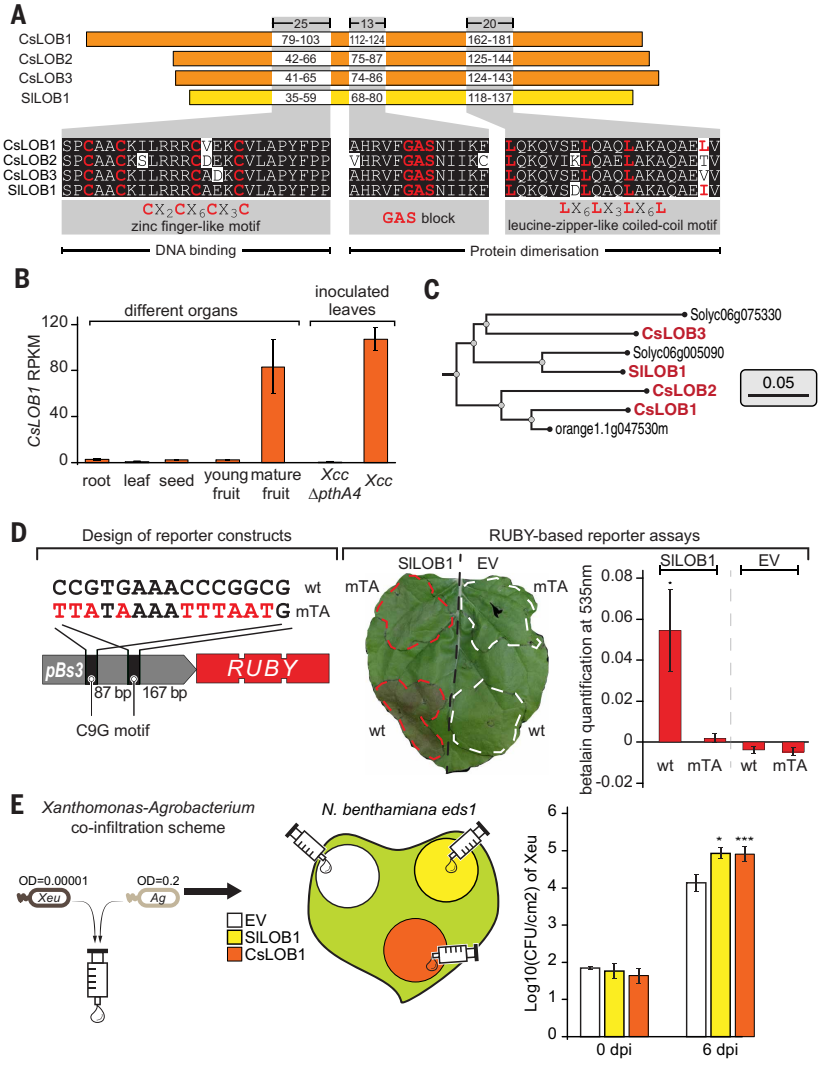

Fig. 3. CsLOB1/2/3 and the tomato ripening regulator homolog SlLOB1 are functionally equivalent. (**A**) LOB domains of CsLOB1/2/3 and SlLOB1. CX2CX6CX3C, cysteine-rich zinc finger-like domain; LX6LX3LX6L, leucine zipper-like domain. Highlights are identical single-letter-code amino acids; red indicates characteristic conserved amino acids; dashed lines indicate domain borders with coordinators. (**B**) *CsLOB1* is high in mature fruit and *Xcc*-infected leaves. RNA-seq data from the Sequence Read Archive (SRA) (*13*) were reanalyzed as in Fig. 1; root *CsLOB1* from citrus HZAU (*14*) due to unavailable raw data. RPKM, reads per kilobase per million mapped reads. Young/mature fruit, 110/312 days after flowering (DAF). (**C**) Phylogeny of tomato and citrus LOB full-length proteins. Full phylogeny and construction are provided in fig. S7A. Branch length, substitutions per site. Scale bar, 0.05. (**D**) SlLOB1 activates a C9G-motif containing promoter. *35S-driven SlLOB1* or EV was codelivered into *N. benthamiana* with RUBY reporter constructs. Betalain was quantified as described in Fig. 2. (**E**) Transient overexpression of *CsLOB1* or *SlLOB1* promotes *Xanthomonas euvesicatoria* (*Xeu*) growth in *N. benthamiana eds1*. Leaves were infiltrated with *Xeu* and *Agrobacterium* carrying *35S:CsLOB1*, *35S:SlLOB1*, or EV (left). Colony-forming units (CFUs) were counted at 0 and 6 dpi ($n = 4$; 2-tailed paired Student's *t* test versus EV, * $P \leq 0.05$, ** $P < 0.001$, error bars indicate SD).

We conducted promoter-GUS reporter assays using the CsLOB1-inducible citrus promoter *Cs5g20320* and the SlLOB1-inducible tomato promoter *SlEXP1* (*18*). When transiently expressed in *N. benthamiana*, both transcription factors activated both the citrus *Cs5g20320* and tomato *SlEXP1* promoters (fig. S7B). SlLOB1 also activated the RUBY reporter driven by a synthetic *Bs3* promoter containing the wt C9G motif, but not by a mutant motif (Figs. 2C and 3D). These results indicate that SlLOB1 recognizes the C9G motif and exhibits similar, if not identical, DNA-binding specificity to CsLOB1/2/3.

CsLOB1 and SlLOB1 promote host susceptibility through cell wall remodeling

Given the similarities with CsLOB1, we expected that ectopic SlLOB1 expression would enhance *Xanthomonas* growth, as seen for CsLOB1 (*6*). We used the immunocompromised *N. benthamiana NbEDS1* mutant, which supports in planta growth of the tomato pathogen *Xanthomonas euvesicatoria* (*Xeu*) (*19*). This system enables *Agrobacterium*-mediated T-DNA delivery into leaves to test how candidate genes affect coinoculated *Xeu*. *Agrobacterium*-mediated expression of CsLOB1 or SlLOB1 in *N. benthamiana* increased *Xeu* growth ~6-fold compared with the empty vector (EV) control at 6 days postinoculation (dpi) (Fig. 3E).

We profiled gene expression in *N. benthamiana* leaves after *Agrobacterium*-mediated expression of *35S:CsLOB1*, *35S:SlLOB1*, or an EV control using RNA-seq. CsLOB1- and SlLOB1-induced transcriptomes clustered together, distinct from EV, indicating similar responses (fig. S8A). The Pearson correlation coefficient ($\rho = 0.765$) confirmed high concordance relative to EV (fig. S8B). In total, 1377 DEGs were shared between CsLOB1 and SlLOB1, representing >50% of the genes induced by each transcription factor. Of these, 346 contained a promoter-proximal, FIMO-predicted C9G promoter motif, suggesting direct targets (fig. S8C). Across shared DEGs, directionally concordant regulation by both transcription factors (fig. S8D) indicates that CsLOB1 and SlLOB1 drive broadly similar transcriptional responses, a similarity likely underestimated by threshold-based DEG overlap alone (fig. S8C).

Together, these findings show that CsLOB1 and SlLOB1 promote *Xeu* proliferation in *N. benthamiana* by activating a shared transcriptional program likely involving C9G-motif genes linked to cell wall remodeling. *N. benthamiana* lacks fleshy fruits, suggesting that CsLOB1/SlLOB1–mediated susceptibility is not strictly dependent on fruit-ripening pathways.

CsLOB1-mediated cell wall breakdown fuels *Xcc* proliferation

We investigated whether CsLOB1 activation alters apoplastic composition to support *Xcc* proliferation. In vitro growth assays showed that *Xcc* grew ~1.5-fold better in filter-sterilized apoplastic fluid from *Xcc*-infected leaves (CsLOB1 induced through PthA4) than in apoplastic fluid from *XccΔpthA4*-infected leaves (CsLOB1 not induced); linear regression confirmed an ~2-fold difference in growth-rate slopes between the two apoplastic fluid sources (see the materials and methods) (Fig. 4A and fig. S9A). We hypothesized that CsLOB1-mediated cell wall degradation releases carbohydrates into the apoplast, supporting *Xcc* growth. Consistent with this, xylose, glucose, fructose, and mannose levels were elevated in apoplastic fluid from *Xcc*-infected leaves compared with controls (Fig. 4B). These findings support a model in which the *Xcc* TALE PthA4 increases apoplastic sugar concentrations, thereby enhancing *Xcc* proliferation. Accordingly, both wt *Xcc* and *XccΔpthA4* should grow similarly in apoplastic fluid from *Xcc*-infected leaves. Indeed, in vitro growth assays showed that apoplastic fluid from *Xcc*-infected leaves supported similar growth of both strains (Fig. 4A and fig. S9A). Thus, PthA4-induced CsLOB1 triggers cell wall breakdown and sugar

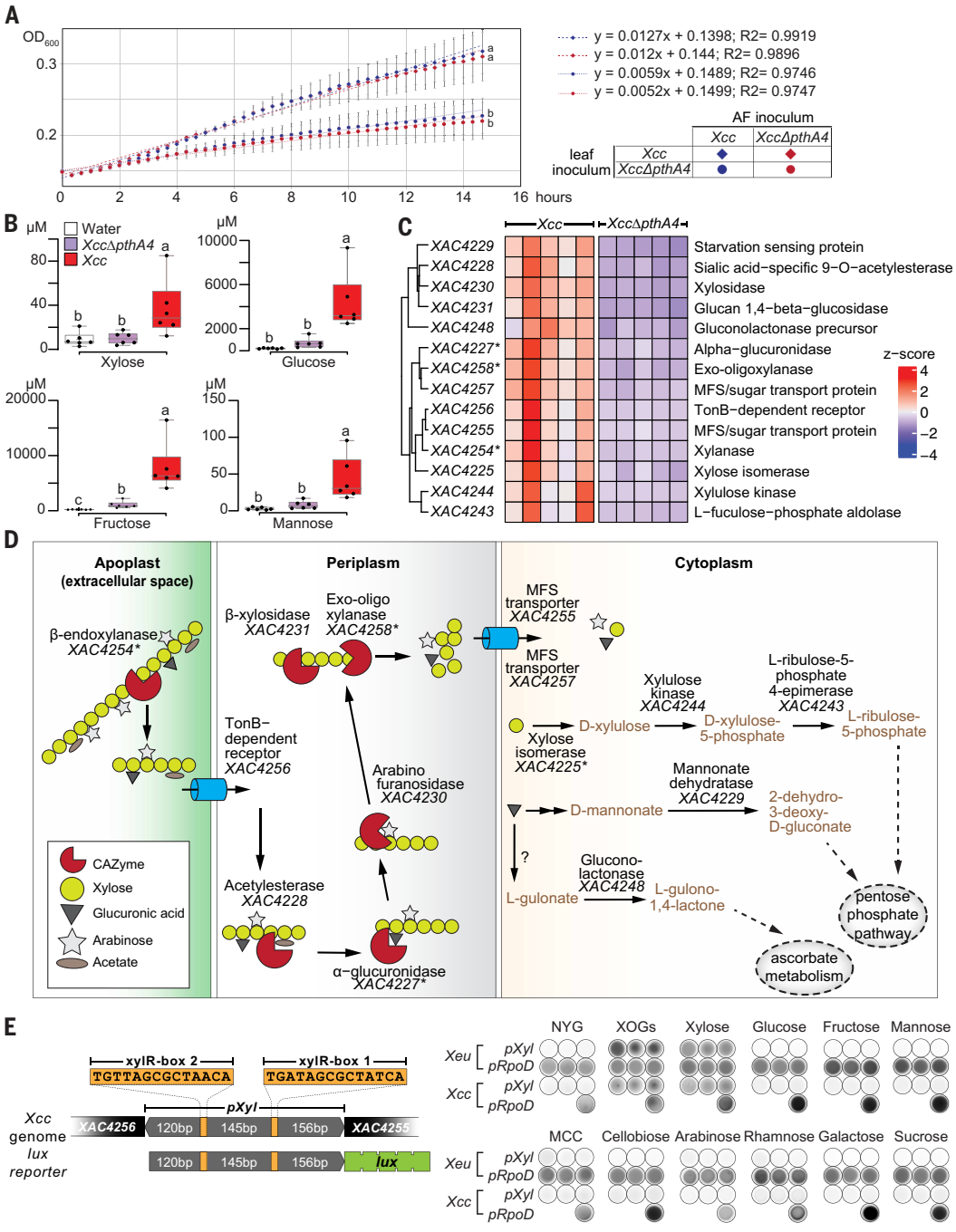

Fig. 4. PthA4 triggers xylose release, activating the xylan degradation regulon in *Xcc*. (**A**) Apoplastic fluids (AFs) from *Xcc*-infected leaves support higher growth of both *Xcc* and *Xcc*Δ*pthA4* versus AFs from *Xcc*Δ*pthA4*-infected leaves. Filter-sterilized AFs recovered at 7 dpi were reinoculated with prewashed *Xcc* or *Xcc*Δ*pthA4*. Growth was assessed by linear regression. Error bars, SD ($n = 4$). End-point values: two-way ANOVA with Tukey's test ($P < 0.05$); same letters indicates not significant. (**B**) Gas chromatography-mass spectrometry (GC-MS) of AFs from (A) revealing increased simple sugars in *Xcc*-infected leaves. Box plots ($n = 6$) show corrected micromolar sugar (median, interquartile range, whiskers = range). Dots indicate individual points. One-way ANOVA with Tukey's test ($P < 0.05$). (**C**) Xylan CUT genes are up-regulated in *Xcc* but not *Xcc*Δ*pthA4* at 5dpi (fig. S9A). Heat map shows transcript level; CUT, carbohydrate-utilization systems associated with TonB-dependent transporters. (**D**) Schematic of *Xcc* xylan CUT enzymes and transporters for xylan degradation. Black arrow indicates direct conversion; double/dashed arrow indicates multienzyme reaction; asterisks indicate previously functionally characterized. (**E**) Xylan-derived metabolites activate xylose-inducible promoter (*pXyl*). Left, *pXyl* in *Xcc* genome and a *pXyl::lux* reporter integrated into *Xeu* and *Xcc* genomes. XylR boxes indicate XylR repressor sites. Right, luminescence after 24 hours on NYG ± sugars; constitutive *pRpoD::lux:* positive control; "spot" indicates independent transconjugant colonies. MCC, microcrystalline cellulose.

release, enabling *Xcc*, including *XccΔpthA4*, to proliferate when these sugars are present.

CUT system expression indicates xylan as the preferred *Xcc* substrate

We sought to determine which cell wall carbohydrate(s) *Xcc* metabolizes to support in planta growth. *Xanthomonas* species encode numerous carbohydrate-active enzymes (CAZymes), many secreted through the T2SS (*20*) and coregulated with TonB-dependent transporter genes. Together, these components form carbohydrate utilization-TonB-dependent transporter (CUT) systems (*21*–*23*). To infer substrate use by *Xcc* versus *XccΔpthA4*, we compared the transcriptomes of in planta–grown bacteria recovered from the citrus apoplast at 5 dpi, when canker symptoms were visible (see the materials and methods) (fig. S9A). This was based on the premise that CUT system expression reflects the substrates a microbe metabolizes (*22*, *24*, *25*). Among 120 PthA4-dependent up-regulated genes (table S5), we identified a CUT system targeting xylan, a hemicellulose composed of β-1,4–linked xylose units (Fig. 4C and fig. S9B). Stepwise xylan degradation was evident from the coordinated functions of CUT system components (Fig. 4D) (*23*, *24*, *26*, *27*). Although CsLOB1 predominantly induces host pectin-degrading enzymes (fig. S5), *Xcc* did not up-regulate pectin-degrading proteins relative to *XccΔpthA4* (table S6) but instead selectively activated a xylan-targeting CUT system.

We generated a polymutant (*XccΔxyl*) lacking three endoxylanases (*XAC4252*, *XAC4254*, and *XAC4249*) and a GH67 α-glucuronidase (*Agu67*; *XAC4227*) that removes 4-O-methyl-D-glucuronic acid side groups from xylan, thereby facilitating backbone cleavage by endoxylanases (see the materials and methods) (fig. S9B) (*24*). Compared with wt *Xcc*, *XccΔxyl* caused milder symptoms and proliferated more slowly in citrus leaves (fig S9, C and D).

Together, these data indicate that CsLOB1-driven *Xcc* proliferation in planta relies on preferential degradation—and utilization—of the hemicellulose xylan.

Release of xylan-derived sugars activates bacterial xylan use

We hypothesized that cell wall–derived sugars serve as metabolic signals that activate xylan CUT-system promoters. To develop a metabolite-responsive promoter-reporter assay, we scanned regions upstream of *xylan CUT* genes. We selected an ~450-bp intergenic region between two divergently transcribed operons, called *pXyl* (Fig. 4E), cloned it upstream of a *lux* reporter operon (*28*), and integrated the construct into the *Xcc* genome (*29*) (Fig. 4E). The resulting *Xcc pXyl::lux* reporter strain was plated on agar supplemented with individual cell wall–derived sugars, including pectin-derived monosaccharides (rhamnose, arabinose, and galactose), cellobiose (the repeating disaccharide unit of cellulose), and xylan-derived sugars [xylose and xylo-oligosaccharides (XOGs)]. Luminescence was induced only by xylose and XOGs (Fig. 4E and fig. S10A), consistent with the observed PthA4/CsLOB1–dependent increase of xylose in apoplastic fluid from *Xcc*-infected leaves (Fig. 4B).

We then investigated whether *pXyl* is induced under physiological conditions. A *pXyl::lux* reporter in *Xeu* showed increased activity during infection of *N. benthamiana* leaves expressing CsLOB1 (fig. S10B), indicating that CsLOB1-dependent *pXyl* activation extends beyond the *Xcc*-citrus pathosystem. To better correlate *pXyl* activation with bacterial density, we incubated the reporter strain in apoplastic fluids harvested from citrus leaves inoculated with either wt *Xcc* or *XccΔpthA4*. Luminescence, normalized to optical density (OD_{600}), was ~2-fold higher in apoplastic fluids from *Xcc*-inoculated leaves, where PthA4 induces CsLOB1, compared with fluids from *XccΔpthA4* infections (fig. S10C). Consistently, these fluids contained higher xylose levels (Fig. 4B). Together, these results support a model in which the *Xcc* effector PthA4 activates CsLOB1 to promote xylan degradation, generating xylose and XOGs that in turn drive expression of the xylan CUT system.

We compared the *Xcc* genomic region comprising five xylose-inducible genes flanking the noncoding *pXyl* region, hereafter referred to as the *pXyl* cluster, with other *Xanthomonas* species. This revealed that *X. oryzae* pv. *oryzae* (*Xoo*), *X. campestris* pv. *campestris* (*Xca*), and *Xeu* share not only an identical arrangement of orthologous genes with *Xcc*, but also high sequence conservation in the *pXyl* region controlling xylose inducibility (fig. S11, A and B). The conserved structure of the *pXyl* cluster across *Xanthomonas* species suggests shared regulatory and functional principles, enabling cross-species insights. The *xytB* locus in *Xca*, which contains these five genes of the *pXyl* cluster, was previously identified as xylose responsive through two 14-bp *XylR* boxes in the *pXyl* region, where the XylR repressor binds to block transcription in the absence of xylose (*30*). These XylR boxes are also conserved in *Xcc*, *Xoo*, and *Xeu* (fig. S11B), suggesting shared XylR-mediated induction through xylose. The five-gene *pXyl* cluster in *Xcc* includes xynB (XAC4254), an endoxylanase with a key role in host cell wall xylan degradation (*26*). Its *Xeu* ortholog, xynB (XCV4360, xynB3), sharing >95% sequence identity, is secreted into the apoplast through the T2SS, and its mutation reduces in planta growth by ~10-fold (*31*).

These results indicate that in *Xcc*, expression of the T2SS-secreted xylanase *xynB* is induced by host-derived xylose, the release of which is triggered by the T3E PthA4. Our work reveals a T3-T2 effector synergy distinct from the prevailing model in which T3Es suppress immune responses triggered by cell wall–degrading T2Es (fig. S12) (*32*, *33*).

Discussion

Our findings suggest that the citrus canker pathogen *Xcc* hijacks a CsLOB1-dependent fruit-ripening program to access cell wall–bound sugars. A key question is the generalizability of this principle, especially in nonfruiting hosts that lack a canonical ripening program. The CsLOB1-dependent increase in *Xanthomonas* growth in the nonfruiting host *N. benthamiana* (Fig. 4E) may be rationalized by the evolutionary history of fruit ripening. Comparative genomics indicates that fleshy-fruit ripening evolved independently across angiosperm lineages by coopting ancestral developmental programs, primarily senescence and abscission, that converge on shared outputs such as CWDE expression (*34*, *35*). Accordingly, the LOB-family transcription factors studied here may link ripening to conserved cell wall–modifying pathways broadly retained across angiosperms.

A key question raised by our study is how the PthA4-triggered ripening program activates the xylose-inducible xylan CUT system in *Xcc*. This program likely releases only limited amounts of xylose, because the induced host proteins lack xylose-releasing xylanases and primarily target pectin, cellulose, and nonxylan hemicelluloses (e.g., mannan), all of which have nonxylose backbones (tables S1 and S4). We speculate that the main benefit of the ripening program for *Xcc* is cell wall loosening, which likely makes cell wall–bound xylan more accessible to degradation by the T2SS-secreted xylanase XynB. XynB-mediated degradation of newly exposed xylan would generate additional xylose, thereby reinforcing CUT system activation. The mechanistic link between a T3E-induced developmental program and T2E activation reveals effector interplay. Our findings challenge the prevailing model of a one-way interaction in which cell wall–degrading T2Es trigger immune responses that are then suppressed by T3Es.

From the pathogen's perspective, hijacking a developmental pathway is a resource-efficient strategy: By deploying a single T3E, *Xcc* activates a regulon of ~100 host genes dedicated to concerted cell wall breakdown. The pathogen exploits not only a preexisting program, but also the host cell's superior biosynthetic capacity, given that plant cells are >1000-fold larger by volume than bacteria. As a result, *Xcc* exerts a disproportionately large effect, likely with only minimal amounts of T3E protein.

Given this efficiency, an open question is whether other T3Es likewise hijack host developmental programs to access cell wall–bound

carbohydrates. Such programs often rely on phytohormones and downstream transcription factors, so the many T3Es known to modulate hormone levels or transcription factor activity (*36*–*38*) may indeed target these regulatory components to gain access to cell wall–bound carbohydrates.

Although apoplastic fluid biochemistry seems straightforward for detecting T3E-induced nutrient changes, proliferating bacteria deplete their preferred carbon sources, thereby limiting the value of such analyses for inferring nutrient availability. Indeed, PthA4-induced xylose accumulation in the apoplast was modest (Fig. 4B), likely due to *Xcc*-mediated consumption. By contrast, transcriptome profiling of in planta–grown bacteria revealed PthA4-dependent induction of the xylan CUT system, a xylose-induced regulon, providing mechanistic insight into how PthA4 promotes *Xcc* growth (Fig. 4, C and D, and fig. S9B). Thus, in planta RNA-seq comparing wt and T3E mutants has strong potential to reveal T3E virulence functions in an unbiased manner.

Our study revealed previously unrecognized fruit-specific expression and regulatory activity of CsLOB1 during ripening, likely overlooked because seed-grown citrus require 5 to 10 years to bear fruit. Identification of the DNA-binding sites of LOB1 ripening regulators in citrus and tomato now enables CRISPR-mediated mutagenesis to modulate LOB1 target gene expression, allowing controlled manipulation of fruit firmness and sweetness in these crops.

REFERENCES AND NOTES

1. D. J. Cosgrove, *Nat. Rev. Mol. Cell Biol.* **25**, 340–358 (2024).
2. A. Molina *et al.*, *Mol. Plant* **17**, 699–724 (2024).
3. A. Molina *et al.*, *Curr. Opin. Plant Biol.* **82**, 102630 (2024).
4. J. D. Jones, J. L. Dangl, *Nature* **444**, 323–329 (2006).
5. J. H. Graham, T. R. Gottwald, J. Cubero, D. S. Achor, *Mol. Plant Pathol.* **5**, 1–15 (2004).
6. Y. Hu *et al.*, *Proc. Natl. Acad. Sci. U.S.A.* **111**, E521–E529 (2014).
7. T. L. Bailey, C. Elkan, *Proc. Int. Conf. Intell. Syst. Mol. Biol.* **2**, 28–36 (1994).
8. R. C. O'Malley *et al.*, *Cell* **165**, 1280–1292 (2016).
9. X. Zou *et al.*, *Plant J.* **106**, 1039–1057 (2021).
10. P. Römer *et al.*, *Science* **318**, 645–648 (2007).
11. Y. He, T. Zhang, H. Sun, H. Zhan, Y. Zhao, *Hortic. Res.* **7**, 152 (2020).
12. J. Zhang *et al.*, *Mol. Plant Pathol.* **18**, 798–810 (2017).
13. L. Ke *et al.*, *Plant J.* **98**, 912–927 (2019).
14. H. Liu *et al.*, *Mol. Plant* **15**, 1503–1505 (2022).
15. G. Feng, J. Wu, Y. Xu, L. Lu, H. Yi, *Plant Biotechnol. J.* **19**, 1337–1353 (2021).
16. B. Buchfink, K. Reuter, H. G. Drost, *Nat. Methods* **18**, 366–368 (2021).
17. H. Huang *et al.*, *Proc. Natl. Acad. Sci. U.S.A.* **116**, 1430–1436 (2019).
18. Y. Shi *et al.*, *Proc. Natl. Acad. Sci. U.S.A.* **118**, e2102486118 (2021).
19. J. Ordon *et al.*, *Plant J.* **89**, 155–168 (2017).
20. C. E. Alvarez-Martinez *et al.*, *Comput. Struct. Biotechnol. J.* **19**, 279–302 (2020).
21. S. Blanvillain *et al.*, *PLOS ONE* **2**, e224 (2007).
22. I. M. Bonfim *et al.*, *Microbiol. Spectr.* **11**, e02280-23 (2023).
23. P. O. Giuseppe, I. M. Bonfim, M. T. Murakami, *Essays Biochem.* **67**, 455–470 (2023).
24. V. Chow *et al.*, *Appl. Environ. Microbiol.* **81**, 2163–2172 (2015).
25. P. S. Vieira *et al.*, *Nat. Commun.* **12**, 4049 (2021).
26. C. R. Santos *et al.*, *J. Biol. Chem.* **289**, 32186–32200 (2014).
27. A. V. Alexandrino *et al.*, *Int. J. Mol. Sci.* **24**, 11491 (2023).
28. C. Gregor, *Sci. Rep.* **12**, 19039 (2022).
29. K. H. Choi, H. P. Schweizer, *Nat. Protoc.* **1**, 153–161 (2006).
30. G. Déjean *et al.*, *New Phytol.* **198**, 899–915 (2013).
31. M. Solé *et al.*, *J. Bacteriol.* **197**, 2879–2893 (2015).
32. D. Sinha, M. K. Gupta, H. K. Patel, A. Ranjan, R. V. Sonti, *PLOS ONE* **8**, e75867 (2013).
33. M. Gravino *et al.*, *Mol. Plant Pathol.* **18**, 582–595 (2017).
34. G. B. Seymour, L. Østergaard, N. H. Chapman, S. Knapp, C. Martin, *Annu. Rev. Plant Biol.* **64**, 219–241 (2013).
35. P. Lü *et al.*, *Nat. Plants* **4**, 784–791 (2018).
36. D. Büttner, *FEMS Microbiol. Rev.* **40**, 894–937 (2016).
37. M. Khan *et al.*, *Microbiol. Res.* **298**, 128220 (2025).
38. K. Kazan, R. Lyons, *Plant Cell* **26**, 2285–2309 (2014).

ACKNOWLEDGMENTS

We thank all members of the Lahaye group, especially A. Strauß, for technical support and helpful discussions; the ZMBP gardeners J. Schröter, P. Becker, and S. Riegger for taking care of the citrus and *N. benthamiana* plants; and E. Ritchie, H. Kim, J. Erickson, and D. Holmes for helpful suggestions and discussions on earlier versions of the manuscript. *NbEDS1* seeds were kindly provided by J. Stuttmann (University of Halle). **Funding:** This work was supported by the Deutsche Forschungsgemeinschaft (DFG grant LA 1338/9-1 to T.L.). Metabolite analytics in the ZMBP Central Facilities unit was also funded by the DFG (project number 442641014). Additional support was provided by the São Paulo Research Foundation (FAPESP grant 2021/04891-3 to M.T.M.). **Author contributions:** Conceptualization: T.L., T.T.-T.P.; Funding acquisition: T.L.; Investigation: T.T.-T.P., R.S.A.S., G.F.P., P.O.G., M.T.M., J.K., P.d.I.A.A., N.W., R.M., J.G., C.L., B.C., B.S., G.V.M., J.B.J.; Methodology: T.T.-T.P., J.K., N.B., C.Liu, P.J.P.L.T.; Project administration: T.L.; Supervision: T.L., T.T.-T.P., E.v.R.-L.; Visualization: T.L., T.T.-T.P.; Writing – original draft: T.L., T.T.-T.P. **Competing interests:** T.L. holds patents on TAL effectors and TAL-effector-responsive promoters in plant disease resistance genes. The remaining authors declare no competing interests. **Data and materials availability:** All data are available in the main text or the supplementary materials. Raw sequencing reads are deposited in the NCBI Sequence Read Archive (SRA) under the following BioProjects: citrus RNA-seq after *Xcc306* infection: PRJNA1345585; citrus ChIP-seq with CsLOB1 antibodies: PRJNA1345397; in planta RNA-seq of *Xcc306* and *Xcc306ΔpthA4*: PRJNA1345539; and *N. benthamiana* RNA-seq: PRJNA1345584. The materials generated in this study are available from the corresponding author upon request.

SUPPLEMENTARY MATERIALS

science.org/doi/10.1126/science.adz9239
Materials and Methods; Figs. S1 to S12; References (*39*–*61*); Data S1 to S9;
MDAR Reproducibility Checklist

Submitted 19 June 2025; accepted 17 October 2025

10.1126/science.adz9239